# Hidden Symmetry and Invariance in Optical Forces

Yikun Jiang,[†,‡,§,∥] Haoze Lin,[†,⊥] Xiao Li,[†,#,○] Jun Chen,[†,□] Junjie Du,[△] and Jack Ng[*,○]

‡State Key Laboratory of Surface Physics, Key Laboratory of Micro and Nano Photonic Structures, and Department of Physics, Fudan University, Shanghai, China

§Collaborative Innovation Center of Advanced Microstructures, Nanjing University, Nanjing, China

∥Department of Physics, Cornell University, Ithaca, New York United States

⊥High School Affiliated to Fudan University, Shanghai, China

#Department of Physics, Hong Kong Baptist University, Hong Kong, China

○Department of Physics, The Hong Kong University of Science and Technology, Hong Kong, China

□Institute of Theoretical Physics and Collaborative Innovation Center of Extreme Optics, Shanxi University, Shanxi, China

△Department of Physics, East China Normal University, Shanghai, China

○Department of Physics, Southern University of Science and Technology, Shenzhen, 518055, China

ⓢ Supporting Information

ABSTRACT: Like any physical quantity whose symmetry properties mimic its source, the optical force acting on a neutral spherical particle has a symmetry that mimics the incident field. The optical force consists of the gradient force and the scattering force. Here, we explicitly show that in optical lattices, the in-plane gradient force and scattering force have additional even and odd symmetries upon $2N$-fold rotation, respectively, which are not shared by the incident field that is N-fold discrete rotationally symmetric. Similar hidden symmetries, namely, even and odd symmetries upon reflection about the focal plane, are also found in particles illuminated by a Gaussian beam, suggesting that it is a general property of the optical force. These are verified numerically in multiple examples and analytically for three incident plane waves, by which we also discover that the profiles of the gradient force and the scattering force are invariant with respect to material composition and particle size for a spherical particle. As such, one can tune the polarization to almost completely "turn off" either gradient force or scattering force, leaving behind a purely irrotational or solenoidal force field, opening a new freedom to control the conservativeness of optical forces.

KEYWORDS: *optical trapping, conservative force, gradient force, nonconservative force, scattering force, optical force decomposition*
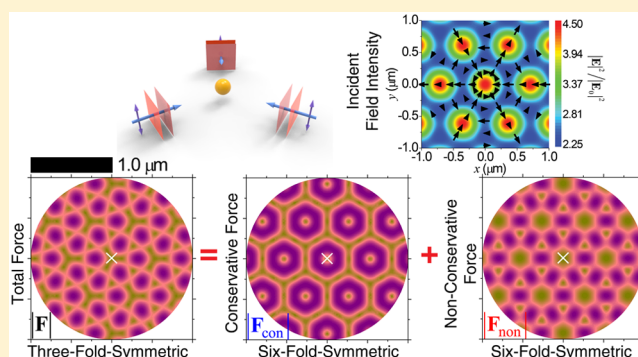
The transfer of photon momentum to physical objects induces optical forces. The most intuitive form is radiation pressure, where light striking a surface exerts a force on it. The investigation of radiation pressure dates back to Kepler, who believed the sun's radiation pressure caused the tail of a comet to point away from the sun. The earliest explanation on a sound mathematical footing, however, was put forward over 200 years later by Maxwell, who established the classical theory of electromagnetism.

The first practical application of optical force was developed by Ashkin in 1970, who successfully trapped and accelerated a micron-sized particle using multiple laser beams.[1] Later, he and co-workers experimentally implemented the optical trapping of a dielectric particle by a single highly focused laser beam,[2] a technique now known as optical tweezers, rating among the most widely recognized applications of optical force. Nowadays, one can achieve a variety of contactless optical micro-manipulations, including optical trapping,[1−19] accelera-tion,[1,20−22] transportation,[23−26] sorting,[27−34] stretching,[35,36] and so on. Indeed, the optical force-based manipulation of microparticles has become an indispensable tool extensively used in physics, chemistry, biology, colloidal science, engineering, and so on.[37−43]

Optical tweezers also mark a milestone in the understanding of light−matter interactions. Scientists have begun to recognize that, besides the radiation pressure, which points along the direction of light propagation, there exists another important optical force, which emerges when an object is put into an inhomogeneous optical field. This force, stemming from the inhomogeneity of the optical field and thus termed the gradient force (GF), does not point along the direction of light propagation in general. For a Rayleigh particle, whose size is
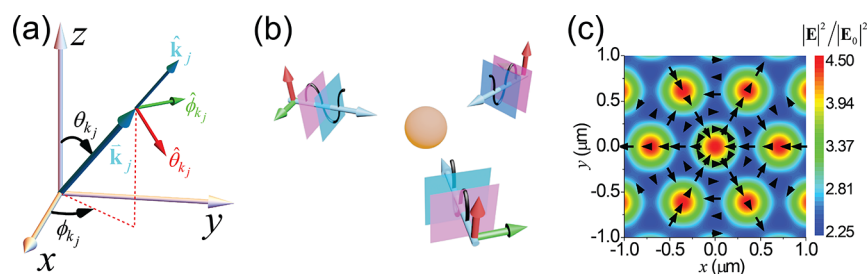
Figure 1. (a) Schematic of the coordinate system. $\hat{k}_j$, $\hat{\theta}_{k_j}$, and $\hat{\phi}_{k_j}$ denote the unit vector triplet for the jth plane wave. (b) Schematic illustration for a sphere illuminated by a TWIF. (c) Contour color plot showing the intensity distribution, while the arrows show the Poynting vector for the TWIF, governed by eqs 2–4, with $(p, q) = (1, i)/\sqrt{2}$, $\lambda = 1.064\ \mu m$, and the background dielectric constant $\varepsilon_b = 1.00$.

much smaller than the illuminating light wavelength, the GF is proportional to the gradient of the free energy, with the proportionality coefficient depending on particle properties such as size, permittivity, and permeability. The remaining part of the optical force is termed the scattering force (SF), of which the previously known radiation pressure is an example.

GF and SF are the two fundamental constituents of the optical force, and they play completely different roles. The curl-less GF, which can be expressed as a gradient of a scalar potential energy, thus conservative, is responsible for optical trapping, by drawing the particle to the intensity maximum (potential minimum) and trapping it therein. The divergence-less SF,[44,45] which typically points in the direction of light propagation, is nonconservative. It also has wide applications, which include propulsion,[25,46,47] pulling,[48−55] light-driven motors,[56−60] and so on, but it cannot trap a particle by itself.[61] Accordingly, dividing the optical force into GF and SF or, in a more physical sense, conservative and nonconservative forces is not only of significance in our understanding of light−matter interaction, but also helps in designing optical fields, as well as the particles being manipulated, to realize a richer diversity of practical application.

The gradient and scattering force components for a Rayleigh particle can be readily separated,[61] while for particles large enough to be considered in the geometrical optics limit, a semianalytical expression of the two force components can also be determined, as their respective light scattering can be determined by Snell's law.[62] Nevertheless, despite the conceptual and practical importance of the GF, for Mie particles, which are the most experimentally accessible, neither a formalism nor any separate and accurate profiles of the GF and SF have emerged after decades of research.[63−65] Until recently, a numerical algorithm based on the Fourier transform was proposed, where the individual profiles of GF and SF acting on a Mie particle were presented for the first time.[66,67] However, the algorithm belongs to a numerical decomposition scheme that is not localized in space (i.e., integration over a very large region is required for convergence) and is, therefore, incapable of obtaining analytical results, thus, obscuring our in-depth physical understanding.

In this Article, we present an alternative algorithm for GF and SF decomposition, which allows semianalytical results for incident light composed of an arbitrary set of plane waves. Because the set of plane waves is complete for propagating waves, this formulation is general. As an illustrative example, we focus on the three-wave interference field (TWIF), which consists of three identical homogeneous plane waves with their wave vectors forming an equilateral triangle, as shown in Figure 1b. The GF and SF acting on a spherical particle residing in such

a field show hidden symmetries that are found in neither the incident field nor the total optical force. In addition, in the TWIF, the profiles of the GF and SF exerted on a spherical particle are solely determined by the optical field itself, while the change of particle properties, such as size and dielectric constant, affects only the magnitude but not the profile of the spatial force. We call this phenomenon profile invariance, which is exclusively true for TWIF illuminating a spherical particle. Finally, to trace the origin of the hidden symmetry and invariant profiles, we derived analytical expressions for the GF and SF acting on a spherical particle of arbitrary size in such a TWIF, which prove explicitly the existence and origin of the hidden symmetry and invariant profiles.

■ RESULTS AND DISCUSSION

Hidden Symmetries in the Gradient and Scattering Force. To see the hidden symmetry, the total optical force (TOF) is decomposed into the conservative irrotational GF and nonconservative solenoidal SF. The time-averaged optical force **F** acting on a particle placed in a monochromatic optical field, denoted simply as the optical force hereafter, can thus be written as

$$\mathbf{F} = \mathbf{F}_{con} + \mathbf{F}_{non} = -\nabla\varphi + \nabla \times \boldsymbol{\psi} \tag{1}$$

where the conservative part (GF) $\mathbf{F}_{con} = -\nabla\varphi$ is expressed as the gradient of a scalar potential φ, and the nonconservative part (SF) $\mathbf{F}_{non} = \nabla \times \boldsymbol{\Psi}$ is written as a curl of a vector potential $\boldsymbol{\Psi}$. The general expressions of both parts are given in ref 68. We explicitly derive the simplified expressions for the case when the optical field is expanded in a discrete set of homogeneous plane waves, as presented in Methods, and these expressions are adopted in this Article.

We consider n_p incident plane waves:

$$\mathbf{E} = E_0 \sum_{j=1}^{n_p} (p_j\hat{\theta}_{k_j} + q_j\hat{\phi}_{k_j})\exp(ik\hat{k}_j \cdot r - i\omega t) \tag{2}$$

where $\hat{k}_j$, $\hat{\theta}_{k_j}$, and $\hat{\phi}_{k_j}$ are the unit vectors in the spherical coordinate system for the jth plane wave, as illustrated in Figure 1. Two complex numbers (p_j, q_j) determine the polarization, and k and ω denote the wavenumber and circular frequency of the waves, respectively.

As an illustrative example, we first consider the TWIF, which is fully characterized by

$$(\theta_{k_1}, \phi_{k_1}) = \left(\frac{\pi}{2}, 0\right), \quad (\theta_{k_2}, \phi_{k_2}) = \left(\frac{\pi}{2}, \frac{2\pi}{3}\right), \quad (\theta_{k_3}, \phi_{k_3}) = \left(\frac{\pi}{2}, \frac{4\pi}{3}\right) \tag{3}$$

and

$$(p_1, q_1) = (p_2, q_2) = (p_3, q_3) = (p, q) \qquad (4)$$

We are interested in the TOF, GF, and SF exerted by the TWIF on a spherical particle immersed therein. Throughout this article, the wavelength is fixed at $\lambda = 1.064\ \mu m$ and the polarization vector (p, q) is normalized such that $|p|^2 + |q|^2 = 1$. The uniform background medium, which does not affect the symmetry, is either water with permittivity $\varepsilon_b = 1.33^2$ or air.

Figure 2 shows the spatial force profiles for a polystyrene particle ($\varepsilon_s = 2.53$) with radius $r_s = 0.3\ \mu m$. Note that Figure 2 is
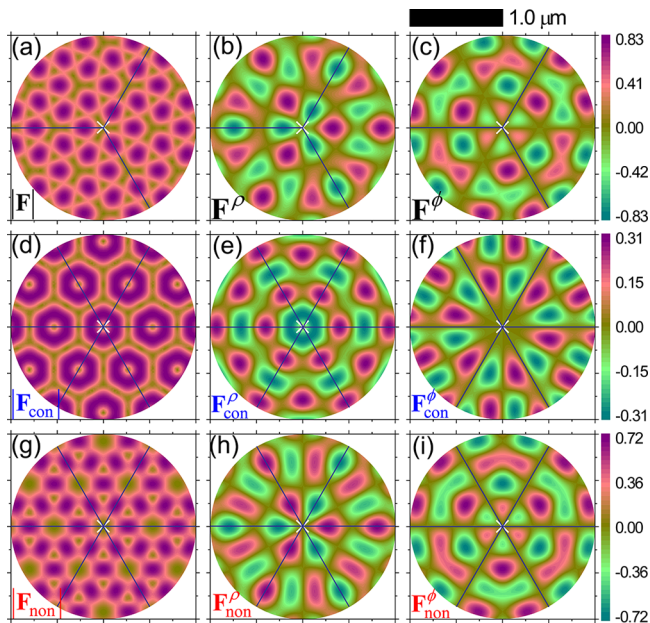
Figure 2. Spatial force profiles for a polystyrene sphere placed in a TWIF. Each point on the figure represents the coordinate of the sphere center. The radius is 0.3 μm and the TWIF has a polarization vector characterized by $(p, q) = (1, i)$. (a–c) The magnitude ($|\mathbf{F}|$), radial part ($\mathbf{F}^\rho = \mathbf{F} \cdot \hat{\boldsymbol{\rho}}$), and azimuthal part ($\mathbf{F}^\phi = \mathbf{F} \cdot \hat{\boldsymbol{\phi}}$) of the total optical force $\mathbf{F}$. (d–f) Same as panels (a)–(c), except that the conservative force $\mathbf{F}_{con}$ is plotted instead of the total optical force. (g–i) Same as panels (a)–(c), except that the nonconservative force $\mathbf{F}_{non}$ is plotted instead of the total optical force. Both conservative and nonconservative forces have additional hidden symmetry that the optical force does not have. GF has a hidden even symmetry, while SF has a hidden odd symmetry. The thin blue lines are guides of eyes to highlight the underlining symmetry.

not showing the force density, rather it plots the optical forces when the sphere is located at different position represented by the horizontal and vertical axes. All plane waves are left-circularly polarized, corresponding to $(p, q) = (1, i)/\sqrt{2}$ in eq 4. Figure 2a–c shows the magnitude of the (undecomposed) TOF and its radial and azimuthal components within the xy-plane to highlight the symmetry. As with the incident fields, the optical force (both radial and azimuthal components) has a 3-fold discrete rotational symmetry and mirror symmetry about the plane formed by $\hat{\mathbf{z}}$ and each $\hat{\mathbf{k}}_j$. No other symmetry can be identified. However, when it is decomposed into the conservative and nonconservative parts, the hidden symmetries are revealed. In addition to the mirror symmetry and the 3-fold discrete rotational symmetry expressed as $\ddot{\mathbf{R}}(2\pi/n_p)\mathbf{F}(\phi) = \mathbf{F}(\phi + 2\pi/n_p)$, Figure 2d–f shows the in-

plane GF, which clearly has what we call a hidden even symmetry, $\ddot{\mathbf{R}}(\pi/n_p)\mathbf{F}_{con}(\phi) = \mathbf{F}_{con}(\phi + \pi/n_p)$, that is absent from the incident field, while Figure 2g–i shows the in-plane SF, which has a hidden odd symmetry, $\ddot{\mathbf{R}}(\pi/n_p)\mathbf{F}_{non}(\phi) = -\mathbf{F}_{non}(\phi + \pi/n_p)$, where $\ddot{\mathbf{R}}$ indicates the rotational matrix with respect to the angles in its argument. In contrast, these symmetries do not exist in the TOF or the incident field. We have performed extensive calculations for particles of different sizes and materials and also for TWIFs with different polarizations and always reached the same conclusion (see Figures S1 and S2), that is, that when the particle size was varied by more than 2 orders of magnitude, the hidden symmetry remained unchanged.

It can be shown that, for an incident field with N-fold discrete rotational symmetries, one has

$$\nabla \cdot \mathbf{F} \propto \nabla \times \mathbf{F} \qquad (5)$$

because

$$\mathbf{F}(\mathbf{r}) = -\frac{1}{4\pi}\nabla \int_V \frac{\nabla' \cdot \mathbf{F}(\mathbf{r}')}{|\mathbf{r} - \mathbf{r}'|}dV' + \frac{1}{4\pi}\nabla \times \int_V \frac{\nabla' \times \mathbf{F}(\mathbf{r}')}{|\mathbf{r} - \mathbf{r}'|}dV' \qquad (6)$$

one can conclude that if the GF has hidden even symmetry, then the SF has hidden odd symmetry. If one assumes that the GF has a hidden even symmetry, which is the case for an optical lattice (Note S3 and Figures S1 and S2), then the SF will have a hidden odd symmetry, in agreement with our calculation. Later in this Article, and also, in Note S2, we prove the existence of these hidden symmetries analytically for a specific incident field. More examples and details are available in the Supporting Information.

Invariant Profiles in the Three-Wave Interference Field. We now proceed to show numerically the invariance of the profiles, that is, that the spatial force profiles of GF and SF acting on a spherical particle immersed in the TWIF are independent of the properties of the particle. In Figure 3a, the
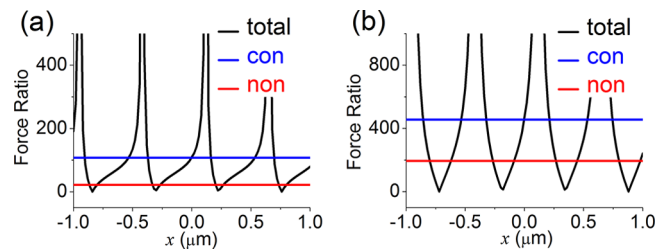
Figure 3. TOF, GF (con), and SF (non) acting on a spherical particle along the x-axis normalized by their corresponding parts in Figure 2, which are at the same positions but with different particles. The particle is illuminated by a TWIF. (a) A spherical particle with $\varepsilon_s = -48.8 + 3.16i$ (silver metal). The radius is 51.5 μm, and the polarization of the TWIF is defined by $(p, q) = (1, 0.5 + i)$ (2/3). (b) A high-dielectric, magnetic particle with $\varepsilon_s = 9$ and $\mu_s = 3$. The radius is $r_s = 42.5\ \mu m$, and the polarization of the TWIF is defined by $(p, q) = (1 - 0.3i, -0.5 + i)$ before normalization.

TOF, GF, and SF at a spatial point on the x-axis acting on a metallic particle with $\varepsilon_s = -48.8 + 3.16i$, $\mu_s = 1$, and $r_s = 51.5\ \mu m$ are divided by the corresponding forces of a 0.3 μm polystyrene sphere located at the same spatial point, while Figure 3b shows the corresponding profiles of a high-dielectric, magnetic particle with $\varepsilon_s = 9$, $\mu_s = 3$, and $r_s = 42.5\ \mu m$. The black line is the TOF, where the drastic variation along the x-axis shows its strong dependence on particle properties. The blue and red curves are the GF and SF, respectively. The curves of divided GF and SF

are flat, which indicates that the force profiles are invariant even when the particle size and composition vary dramatically, as in Figure 3. Nevertheless, the magnitudes of the GF and SF depend drastically (and differently) on the particle properties. As a result, when the GF and SF are combined into the TOF, the profile is no longer independent of the particle properties, as shown by the black line. In addition, the spatial profiles of both GF and SF are independent of the incident polarization (data not shown). The profile invariance of the GF and SF is proved analytically in a later part of the article, as well as in Note S2. Further examples and details can be found in Figures S1 and S2.

Analytical Proof of the Hidden Symmetry and Invariant Profiles. To trace the origin of the hidden symmetry and profile invariance, we derived rigorous analytical expressions for the optical force acting on a spherical particle placed in a TWIF. The particle can be of arbitrary size and made from any isotropic and homogeneous material. The mathematical results are summarized in Note S2. In short, it is derived rigorously and analytically that in a TWIF

$$\mathbf{F}_{con} \propto \nabla |\mathbf{E}|^2,$$

$$(\mathbf{F}_{non})_{\parallel} \propto \mathrm{Re}(\mathbf{E} \times \mathbf{B}^*)_{\parallel}, \tag{7}$$

for any homogeneous and isotropic particles, where $\parallel$ indicates the transverse components on the xy-plane. Accordingly, as evident from Figure 1b,c, in addition to the 3-fold discrete rotational symmetry and the $\hat{\mathbf{k}}_j$–$\hat{\mathbf{z}}$-plane mirror symmetry of the incident field, the GF has a hidden even symmetry, while the SF has an additional hidden odd symmetry.

For the TWIF, the spatial force profiles for the GF and SF are invariant with respect to polarization as well as particle properties. We remark that while profile invariance is a unique property of the TWIF, hidden symmetry is a general physical phenomenon that can be found in many situations.

Generating Conservative or Nonconservative Force Fields. We can thus design appropriate optical fields by simply tuning the polarization vector $(p, i\sqrt{1-p^2})$ such that a given particle is subject exclusively to either conservative GF or nonconservative SF. Figure 4a−c shows a phase diagram for a particle of radii equal to 0.5λ, 1.0λ, and 1.5λ, respectively. The green and blue regions correspond to areas in the ε−μ phase space, where one can tune p to induce nearly conservative and nearly nonconservative forces (in-plane), respectively. We note that, in experiments, the z-direction force can be counterbalanced by another force. For example, each incident wave can have a small upward component in its k-vector, which pushes the particle against a substrate, hence, stabilizing the z-directional motion. The conservative force can be more than 3 orders of magnitude larger than the nonconservative force, and vice versa. The red parts in Figure 4 denote regions where the relative strength of the two forces can be varied from $\sim 10^{-3}$ to $\sim 10^3$ by simply tuning p. The situations denoted by the various colors are summarized in Figure 4d. This system allows one to switch between a conservative and a nonconservative phase readily. It is difficult to realize purely conservative or nonconservative force for larger particles, as the colored regions gradually shrink with increasing radius, especially for the green regime. Figure 5a shows a phase diagram in the permittivity−radius space. One observes that with $r_s \lesssim 0.25\lambda$, one can tune p such that the conservative force becomes dominant. As the particle size increases, it becomes harder to achieve a nearly conservative force, at least with a TWIF. However, it becomes easier to make
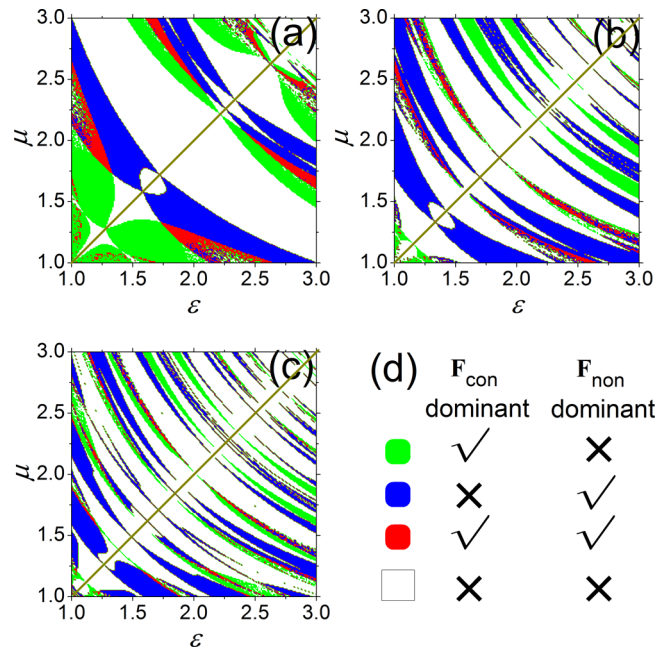

Figure 4. Phase diagrams in the permittivity−permeability space for optical forces acting on a particle of radius 0.5λ (a), 1.0λ (b), and 1.5λ (c), illuminated by a TWIF in air. Green (blue) regions denote combinations of ε and μ at which extremely dominant conservative (nonconservative) force can be realized by tuning the value of p in the polarization vector, where $(p, q) = (p, i\sqrt{1-p^2})$. Here "extremely dominant" means one of the forces is greater than the other by at least 3 orders of magnitude. In the red regions, one can achieve both extremely dominant conservative and nonconservative forces. The diagonal straight lines are guides to the eye to illustrate the symmetry with respect to ε and μ. (d) Color key to the tunability of conservative and nonconservative forces.

the nonconservative force dominant, as the blue color encompasses most of the phase space, while the main part of the green regime appears near the low-permittivity region for large particles, except for some small scattered regions. Figure 5b is an enlarged version of the shaded part in Figure 5a. The two straight lines cross at the red point in Figure 5b, which has $\varepsilon = 2.0$ and $r_s = 0.85\lambda$, serving as a typical example for the case in which, by tailoring p, one can switch the optical force from nearly conservative to nearly nonconservative. The case is visualized more clearly in Figure 5c−f. In polarization 1, shown in Figure 5c,d, the nonconservative force is 4 orders of magnitude larger, while conversely in polarization 2 (Figure 5e,f), the conservative force is larger, again by 4 orders of magnitude.

We note that, for optical lattices other than a TWIF, one can also switch between the conservative and nonconservative phases by tuning the polarization. Figure 6 shows the forces for a quasi-crystal optical lattice formed by five-wave interference (with 5-fold discrete rotationally symmetric fields). The regime where the conservative force dominates is illustrated in Figure 6a−c, where the profiles of TOF and GF are nearly the same. Likewise, the nonconservative-dominated regime is illustrated in Figure 6g−i, where the profiles of TOF and SF are nearly the same. An intermediate case where GF and SF are comparable is shown in Figure 6d−f. In addition to the 5-fold rotational symmetry and mirror symmetry possessed by the incident field and TOF, the GF and SF clearly have additional hidden even or odd symmetry.
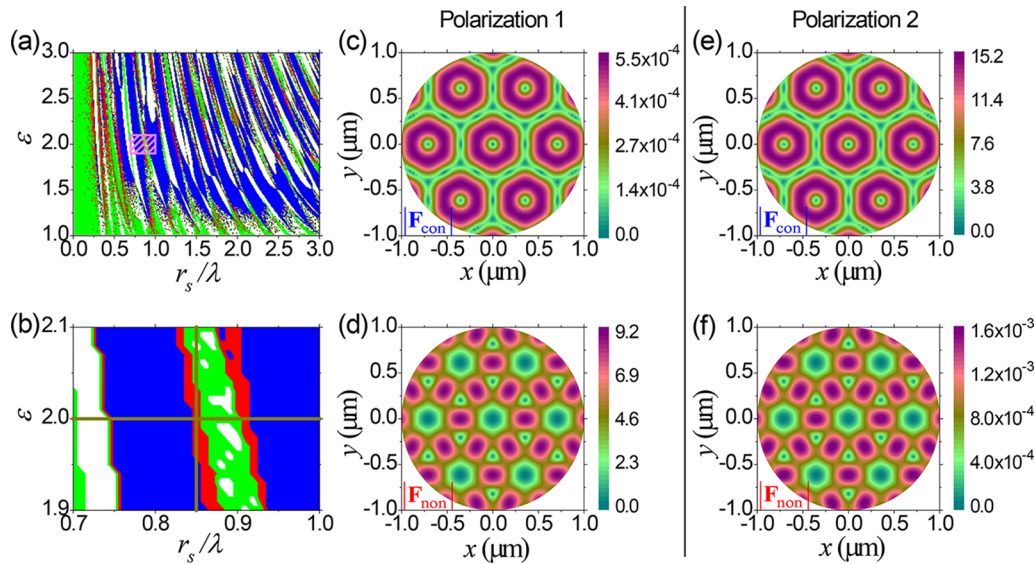
Figure 5. (a) Similar to Figure 4, but in the radius−permittivity phase space. (b) An enlarged view of the shaded part in panel (a). The two straight yellow lines cross at a red point with $\varepsilon = 2.0$ and $r_s = 0.85\lambda$, where both dominant conservative and dominant nonconservative optical forces can be achieved by tuning the value of p. (c, d) The spatial distribution profiles of conservative forces acting on a particle with $\varepsilon = 2.0$ and $r_s = 0.85\lambda$ sitting in the TWIF with polarization vector $(p, q) = (p, i\sqrt{1 - p^2})$, with $p = 0.153$. A nearly pure nonconservative force is observed over the entire space, outweighing its conservative counterpart by over 3 orders of magnitude. (e, f) The same as panels (c) and (d), except for $p = 0.745$. Now the conservative force surpasses its counterpart by over 3 orders of magnitude. Panels (c)−(f) suggest a simple procedure to switch between two essentially different optical forces through tuning the polarization of the incident wave.
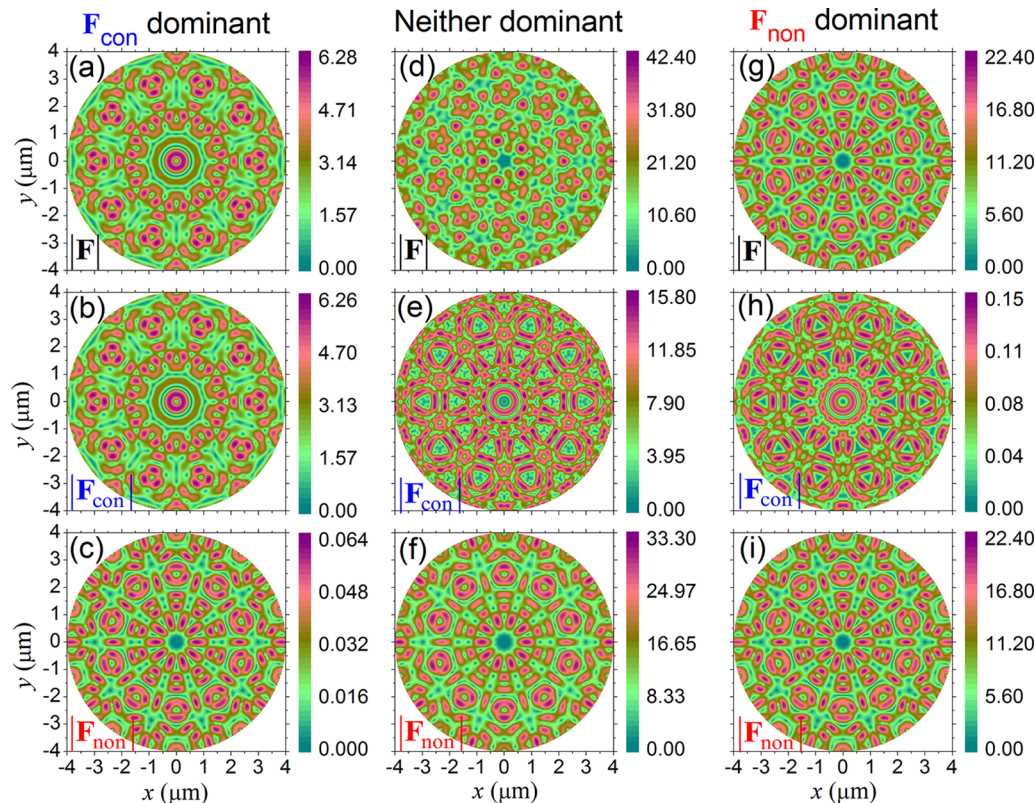
Figure 6. Forces acting on a dielectric particle induced by a quasi-crystal optical lattice formed by five identical plane waves with their wave vectors forming a regular pentagon in air. (a−c) A situation ($r_s = 0.45\lambda$, $\varepsilon = 1.25$, and $(p, q) = (0.6625, 0.7491i)$) where $\mathbf{F}_{con}$ dominates. (d−f) A situation ($r_s = 0.50\lambda$, $\varepsilon = 2.50$, and $(p, q) = (1, i)/\sqrt{2}$) where neither dominant. (g)−(i) show the situation ($r_s = 0.50\lambda$, $\varepsilon = 2.00$, and $(p, q) = (0.7, 0.7141i)$), where $\mathbf{F}_{non}$ dominates.

Although one cannot completely eliminate either the GF or the SF, their strengths can differ by 2−3 orders of magnitude, as shown in Figures 5 and 6, suggesting a convenient and effective way to create conservative or nonconservative force fields by

simply tuning the polarization. It is noted again that the GF and SF keep their hidden symmetry, regardless of changes in the polarization and particle properties.

In the additional supporting files, we include four movies (Movies 1, 2, 3, and 4) to illustrate how the phase diagrams in the permittivity−permeability space evolve for particles with varying radius. One can easily identify parameter combinations in which either $\mathbf{F}_{con}$ or $\mathbf{F}_{non}$ is dominant, both are dominant, or neither is dominant.

■ CONCLUSIONS

We have proved, numerically and analytically, that the GF and SF have hidden symmetries, where the incident field and TOF do not. Creating a TWIF allows the GF and SF to have higher symmetry than the incident field and TOF, indicating a different origin for these forces. According to eq 7, the GF is dictated by the gradient of the intensity, and thus, its hidden symmetry is even, whereas the SF is proportional to the Poynting vector and its hidden symmetry is odd. We stress that eq 7, derived for TWIF, is exact for a particle of arbitrary size rather than only valid under small particle approximation.

A simple method is proposed to tune a force field to be nearly conservative or nonconservative by varying the polarization, which works for crystal or quasi-crystal optical lattices. We note that it is formally incorrect to treat an optical lattice such as the TWIF as a 3-fold discrete rotationally symmetric potential for dielectric particles, even approximately, because its conservative part is 6-fold symmetric for spherical particle of arbitrary size, even though it is not simply proportional to the gradient of light intensity.

Last but not least, we remark that hidden symmetries like those for the optical lattices also exist for a sphere trapped by ideal water-immersed optical tweezers, which assumes an aplanatic beam with no aberration, as supported by analyzing the data presented in ref 66. The GF in aberration-free optical tweezers is found to have an odd symmetry (defined by $\mathbf{F}_{con}^x(x,y,z) = -\mathbf{F}_{con}^x(-x,y,z)$, $\mathbf{F}_{con}^y(x,y,z) = -\mathbf{F}_{con}^y(x,-y,z)$, and $\mathbf{F}_{con}^z(x,y,z) = -\mathbf{F}_{con}^z(x,-y,z)$), which is also true for the transverse SF ($\mathbf{F}_{non}^x$ and $\mathbf{F}_{non}^y$). However, the longitudinal SF, $\mathbf{F}_{non}^z$, has an even symmetry (defined by $\mathbf{F}_{non}^z(x,y,z) = -\mathbf{F}_{non}^z(x,y,-z)$), as shown in Figure S5. In summary, hidden symmetries exist in high-symmetry situations and can take different forms such as hidden even and hidden odd rotational symmetries and hidden even and hidden odd mirror symmetries.

■ METHODS

Decomposing the Optical Force into Conservative and Nonconservative Components. The general formulation for partitioning the optical force into the conservative (GF) and nonconservative (SF) parts was previously derived.[68] Here we give a somewhat more straightforward formalism for the case when the optical field is expanded by a discrete set of homogeneous plane waves, which is applicable for any monochromatic field, at least in principle.

By expanding the incident electric field in plane waves, one arrives at

$$\mathbf{E} = \sum_{i=1}^{n_p} \mathbf{E}_i \quad \text{with} \quad \mathbf{E}_i = E_0 \mathcal{E}_i \exp(i k_i \cdot r) \quad (8)$$

where $\mathcal{E}_i = (p_i \hat{\theta}_{k_i} + q_i \hat{\phi}_{k_i})$ is the complex vector amplitude for the ith plane wave, and the time dependence $\exp(-i\omega t)$ has been

assumed and skipped for simplicity. The (time-averaged) optical force $\mathbf{F}$ acting on a spherical particle immersed in such an optical field is written as a sum of the interception force $\mathbf{F}_{int}$ and recoil force $\mathbf{F}_{rec}$:[48]

$$\mathbf{F}_{int} = \mathbf{F}_{int}^e + \mathbf{F}_{int}^m,$$

$$\mathbf{F}_{rec} = \mathbf{F}_{rec}^e + \mathbf{F}_{rec}^m + \mathbf{F}_{rec}^x \quad (9)$$

where each term consists of a sum over various orders of electric and magnetic multipoles. Their full explicit expressions can be found in Note S1. As an example, we present below the electric part of the interception force $\mathbf{F}_{int}^e$, which reads, in electrodynamic units with $c = \varepsilon_0 = \mu_0 = 1$:

$$\mathbf{F}_{int}^e = \sum_{l=1}^{\infty} \mathbf{F}_{int}^{e(l)},$$

$$\mathbf{F}_{int}^{e(l)} = -\frac{\pi E_0^2(2l+1)}{2l(l+1)} \text{Im} \sum_{i=1}^{n_p} \sum_{j=1}^{n_p} a_l [Q_l^{(1)}(x_{i,j}) \mathbf{Z}_{i,j}^{ee} - Q_l^{(2)}(x_{i,j}) \mathbf{Z}_{i,j}^{mm}] \quad (10)$$

where a_l is the Mie coefficient,[69] n_p is the number of plane waves that make up the optical field, and $x_{i,j} = \hat{\mathbf{k}}_i \cdot \hat{\mathbf{k}}_j$. Two auxiliary functions, $Q_l^{(1)}(x)$ and $Q_l^{(2)}(x)$, can be expanded in the Legendre polynomials $P_n(x)$:

$$Q_l^{(1)}(x) = \sum_{m=1}^{(2)\,l} m(2l+1-m)(2l+1-2m)P_{l-m}(x),$$

$$Q_l^{(2)}(x) = \sum_{m=2}^{(2)\,l} m(2l+1-m)(2l+1-2m)P_{l-m}(x) \quad (11)$$

with $\sum_{m=1}^{(2)\,l}$ and $\sum_{m=2}^{(2)\,l}$ denoting that the summation index m assumes, respectively, all positive odd and even integers between 1 and l. In eq 10, each of the two auxiliary vectors $\mathbf{Z}_{i,j}^{ee}$ and $\mathbf{Z}_{i,j}^{mm}$ is separated into a gradient term and two remainder terms that contribute only to the solenoidal parts,

$$\mathbf{Z}_{i,j}^{ee} = \nabla D_{i,j}^{ee} - \nabla \times \mathbf{S}_{i,j}^{ee} - 2i\text{Re}\mathbf{S}_{i,j}^{em},$$

$$\mathbf{Z}_{i,j}^{mm} = \nabla D_{i,j}^{mm} - \nabla \times \mathbf{S}_{i,j}^{mm} - 2i\text{Re}\mathbf{S}_{i,j}^{em} \quad (12)$$

with

$$D_{i,j}^{ee} = \mathcal{E}_i \cdot \mathcal{E}_j^* \exp[i(k_i - k_j)\cdot r], \quad D_{i,j}^{mm} = \mathcal{B}_i \cdot \mathcal{B}_j^* \exp[i(k_i - k_j)\cdot r],$$

$$\mathbf{S}_{i,j}^{ee} = \mathcal{E}_i \times \mathcal{E}_j^* \exp[i(k_i - k_j)\cdot r], \quad \mathbf{S}_{i,j}^{mm} = \mathcal{B}_i \times \mathcal{B}_j^* \exp[i(k_i - k_j)\cdot r],$$

$$\mathbf{S}_{i,j}^{em} = \mathcal{E}_i \times \mathcal{B}_j^* \exp[i(k_i - k_j)\cdot r] \quad (13)$$

and $\mathbf{B}_i = k_i \times \mathbf{E}_i$. It can be proved that the term associated with $\text{Re}\mathbf{S}_{i,j}^{em}$ in eq 12 makes no contribution to the conservative part of the optical force. It is noted that in all ∇ one should replace $\partial/\partial x_i$ by $\partial/\partial(kx_i)$. Hence, eqs 10−13 complete the decomposition of the electric part of the interception force $\mathbf{F}_{int}^e$. To be more specific, replacing vectors $\mathbf{Z}_{i,j}^{ee}$ and $\mathbf{Z}_{i,j}^{mm}$ by their real parts, $\text{Re}[\mathbf{Z}_{i,j}^{ee}]$ and $\text{Re}[\mathbf{Z}_{i,j}^{mm}]$, respectively, in eq 10 gives the conservative part $\mathbf{F}_{int,con}^e$, while substituting $\text{Im}[\mathbf{Z}_{i,j}^{ee}]$ and $\text{Im}[\mathbf{Z}_{i,j}^{mm}]$ for $\mathbf{Z}_{i,j}^{ee}$ and $\mathbf{Z}_{i,j}^{mm}$ leaves us with the nonconservative part $\mathbf{F}_{int,non}^e$ of the electric part of the interception force. The treatment of the other terms in eq 9 is similar but mathematically more complicated (see Note S1).

It is noted that

$$\sum_{i=1}^{n_p} \sum_{j=1}^{n_p} \nabla D_{i,j}^{ee} = \nabla |\mathbf{E}|^2, \quad \sum_{i=1}^{n_p} \sum_{j=1}^{n_p} \nabla D_{i,j}^{mm} = \nabla |\mathbf{B}|^2,$$

$$\sum_{i=1}^{n_p} \sum_{j=1}^{n_p} \nabla \times \mathbf{S}_{i,j}^{ee} = \nabla \times (\mathbf{E} \times \mathbf{E}^*), \quad \sum_{i=1}^{n_p} \sum_{j=1}^{n_p} \nabla \times \mathbf{S}_{i,j}^{mm} = \nabla \times (\mathbf{B} \times \mathbf{B}^*),$$

$$\sum_{i=1}^{n_p} \sum_{j=1}^{n_p} \mathbf{S}_{i,j}^{em} = (\mathbf{E} \times \mathbf{B}^*)$$

$$(14)$$

which are associated with the gradient of light density, the curl of the spin angular momentum density (also known as Belinfante spin density), and the complex Poynting vector, as well as some constant factors.

Some Relations in the TWIF. In the TWIF described by eqs 2−4, it is straightforward to demonstrate that

$$(3|q|^2 - 2)\nabla|\mathbf{B}|^2 = (3|p|^2 - 2)\nabla|\mathbf{E}|^2$$

$$\nabla \times (\mathbf{E} \times \mathbf{E}^*) = \begin{cases} -3i|q|^2 \mathrm{Re}(\mathbf{E} \times \mathbf{B}^*)_\parallel, & \text{for } x \text{ or } y \text{ component} \\ -2i\mathrm{Re}(\mathbf{E} \times \mathbf{B}^*)_\perp, & \text{for } z \text{ component} \end{cases}$$

$$\nabla \times (\mathbf{B} \times \mathbf{B}^*) = \begin{cases} -3i|p|^2 \mathrm{Re}(\mathbf{E} \times \mathbf{B}^*)_\parallel, & \text{for } x \text{ or } y \text{ component} \\ -2i\mathrm{Re}(\mathbf{E} \times \mathbf{B}^*)_\perp, & \text{for } z \text{ component} \end{cases}$$

$$\mathrm{Im}(\mathbf{E} \times \mathbf{B}^*) = \begin{cases} \frac{1}{3}(\nabla|\mathbf{E}|^2 - \nabla|\mathbf{B}|^2)_\parallel, & \text{for } x \text{ or } y \text{ component} \\ \frac{\mathrm{Re}(pq^*)}{\mathrm{Im}(pq^*)}\mathrm{Re}(\mathbf{E} \times \mathbf{B}^*)_\perp, & \text{for } z \text{ component} \end{cases}$$

$$(15)$$

It is noteworthy that, while $\mathrm{Re}(\mathbf{E} \times \mathbf{B}^*)$ is purely solenoidal, $\mathrm{Im}(\mathbf{E} \times \mathbf{B}^*)$ contains an irrotational component parallel to the plane formed by the three wave vectors and a solenoidal component perpendicular to the wave vector plane. When $\mathrm{Im}(pq^*) = 0$, one has an identically vanishing $\mathrm{Re}(\mathbf{E} \times \mathbf{B}^*)$ and a finite $\mathrm{Im}(\mathbf{E} \times \mathbf{B}^*)$.

■ ASSOCIATED CONTENT

Ⓢ Supporting Information

The Supporting Information is available free of charge on the ACS Publications website at DOI: 10.1021/acsphotonics.9b00746.

Movie S1: Three plane waves (AVI)
Movie S2: Five plane waves (AVI)
Movie S3: Seven plane waves (AVI)
Movie S4: Nine plane waves (AVI)
Supporting notes, figures and tables (PDF)

■ AUTHOR INFORMATION

Corresponding Author

*E-mail: wuzh3@sustech.edu.cn.

ORCID 🅞

Xiao Li: 0000-0001-6273-0621

Author Contributions

[†]These authors contributed equally to this work. All authors discussed the physics thoroughly. Y.J. derived most of the formalism for conservative and nonconservative optical forces. J.C. assisted in the derivation and wrote the code together with H.L. H.L. and J.C. performed part of the simulations and discovered the key phenomena. X.L. performed most of the simulations and derived the rigorous explicit expressions of optical force to analytically demonstrate the key phenomena.

J.D. assisted in writing code and performed part of the simulations. J.N. initiated and oversaw the project. The manuscript was written by J.N, X.L., and J.D.

Notes

The authors declare no competing financial interest.

■ REFERENCES

(1) Ashkin, A. Acceleration and trapping of particles by radiation pressure. *Phys. Rev. Lett.* **1970**, *24*, 156.

(2) Ashkin, A.; Dziedzic, J. M.; Bjorkholm, J. E.; Chu, S. Observation of a single-beam gradient force optical trap for dielectric particles. *Opt. Lett.* **1986**, *11*, 288−290.

(3) Chu, S.; Bjorkholm, J. E.; Ashkin, A.; et al. Experimental observation of optically trapped atoms. *Phys. Rev. Lett.* **1986**, *57*, 314.

(4) Ashkin, A.; Dziedzic, J. M.; Yamane, T. Optical trapping and manipulation of single cells using infrared laser beams. *Nature* **1987**, *330*, 769.

(5) Ashkin, A.; Dziedzic, J. M. Optical trapping and manipulation of viruses and bacteria. *Science* **1987**, *235*, 1517−1520.

(6) Gahagan, K. T.; Swartzlander, G. A. Optical vortex trapping of particles. *Opt. Lett.* **1996**, *21*, 827−829.

(7) Ng, J.; Lin, Z. F.; Chan, C. T. Theory of optical trapping by an optical vortex beam. *Phys. Rev. Lett.* **2010**, *104*, 103601.

(8) Lee, S. H.; Roichman, Y.; Grier, D. G. Optical solenoid beams. *Opt. Express* **2010**, *18*, 6988−6993.

(9) Svoboda, K.; Block, S. M. Optical trapping of metallic Rayleigh particles. *Opt. Lett.* **1994**, *19*, 930−932.

(10) Grzegorczyk, T. M.; Kemp, B. A.; Kong, J. A. Stable optical trapping based on opticalbinding forces. *Phys. Rev. Lett.* **2006**, *96*, 113903.

(11) Taylor, M. A.; Waleed, M.; Stilgoe, A. B.; Rubinsztein-Dunlop, H.; Bowen, W. P. Enhancedoptical trapping via structured scattering. *Nat. Photonics* **2015**, *9*, 669−673.

(12) Dufresne, E. R.; Spalding, G. C.; Dearing, M. T.; Sheets, S. A.; Grier, D. G. Computer-generatedholographic optical tweezer arrays. *Rev. Sci. Instrum.* **2001**, *72*, 1810−1816.

(13) Righini, M.; Zelenina, A. S.; Girard, C.; Quidant, R. Parallel and selective trapping in apatterned plasmonic landscape. *Nat. Phys.* **2007**, *3*, 477−480.

(14) Juan, M. L.; Gordon, R.; Pang, Y. J.; Eftekhari, F.; Quidant, R. Self-induced back-action opticaltrapping of dielectric nanoparticles. *Nat. Phys.* **2009**, *5*, 915−919.

(15) Zhao, Y.; Saleh, A. A. E.; Dionne, J. A. Enantioselective optical trapping of chiral nanoparticleswith plasmonic tweezers. *ACS Photonics* **2016**, *3*, 304−309.

(16) Zhang, W. H.; Huang, L. N.; Santschi, C.; Martin, O. J. F. Trapping and sensing 10 nm metalnanoparticles using plasmonic dipole antennas. *Nano Lett.* **2010**, *10*, 1006−1011.

(17) Li, Y. C.; Xin, H. B.; Liu, X. S.; Zhang, Y.; Lei, H. X.; et al. Trapping and detection ofnanoparticles and cells using a parallel photonic nanojet array. *ACS Nano* **2016**, *10*, 5800−5808.

(18) Woerdemann, M.; Alpmann, C.; Esseling, M.; Denz, C. Advanced optical trapping bycomplex beam shaping. *Laser Photon. Rev.* **2013**, *7*, 839−854.

(19) Maragò, O. M.; Jones, P. H.; Gucciardi, P. G.; Volpe, G.; Ferrari, A. C. Optical trapping andmanipulation of nanostructures. *Nat. Nanotechnol.* **2013**, *8*, 807−819.

(20) Shalin, A. S.; Sukhov, S. V. Plasmonic nanostructures as accelerators for nanoparticles: optical nanocannon. *Plasmonics* **2013**, *8*, 625−629.

(21) Maher-McWilliams, C.; Douglas, P.; Barker, P. F. Laser-driven acceleration of neutral particles. *Nat. Photonics* **2012**, *6*, 386.

(22) Barker, P. F.; Shneider, M. N. Optical microlinear accelerator for molecules and atoms. *Phys. Rev. A: At., Mol., Opt. Phys.* **2001**, *64*, 033408.

(23) Ndukaife, J. C.; Kildishev, A. V.; Nnanna, A. G. A.; Shalaev, V. M.; Wereley, S. T.; et al. Long-rangeand rapid transport of individual nano-objects by a hybrid electrothermoplasmonicnanotweezer. *Nat. Nanotechnol.* **2016**, *11*, 53–59.

(24) Ruffner, D. B.; Grier, D. G. Optical conveyors: a class of active tractor beams. *Phys. Rev. Lett.* **2012**, *109*, 163903.

(25) Čižmar, T.; Garces-Chavez, V.; Dholakia, K.; Zemanek, P. Optical conveyor belt for deliveryof submicron objects. *Appl. Phys. Lett.* **2005**, *86*, 174101.

(26) Baumgartl, J.; Mazilu, M.; Dholakia, K. Optically mediated particle clearing using Airywavepackets. *Nat. Photonics* **2008**, *2*, 675–678.

(27) Almaas, E.; Brevik, I. Possible sorting mechanism for micro-particles in anevanescent field. *Phys. Rev. A: At., Mol., Opt. Phys.* **2013**, *87*, 063826.

(28) Wang, M. M.; Tu, E.; Raymond, D. E.; Yang, J. M.; Zhang, H.; et al. Microfluidic sorting ofmammalian cells by optical force switching. *Nat. Biotechnol.* **2005**, *23*, 83–87.

(29) Roxworthy, B. J.; Ko, K. D.; Kumar, A.; Fung, K. H.; Chow, E. K. C.; et al. Application of plasmonicbowtie nanoantenna arrays for optical trapping, stacking, and sorting. *Nano Lett.* **2012**, *12*, 796–801.

(30) Paterson, L.; Papagiakoumou, E.; Milne, G.; Garces-Chavez, V.; Tatarkova, S. A.; et al. Light-inducedcell separation in a tailored optical landscape. *Appl. Phys. Lett.* **2005**, *87*, 123901.

(31) Zemanek, P.; Karasek, V.; Sasso, A. Optical forces acting on Rayleigh particle placed intointerference field. *Opt. Commun.* **2004**, *240*, 401–415.

(32) Zelenina, A. S.; Quidant, R.; Badenes, G.; Nieto-Vesperinas, M. Tunable optical sortingand manipulation of nanoparticles via plasmon excitation. *Opt. Lett.* **2006**, *31*, 2054–2056.

(33) Pelton, M.; Ladavac, K.; Grier, D. G. Transport and fractionation in periodic potentialenergylandscapes. *Phys. Rev. E* **2004**, *70*, 031108.

(34) Korda, P. T.; Taylor, M. B.; Grier, D. G. Kinetically locked-in colloidal transport in anarray of optical tweezers. *Phys. Rev. Lett.* **2002**, *89*, 128301.

(35) Guck, J.; et al. Optical deformability of soft biological dielectrics. *Phys. Rev. Lett.* **2000**, *84*, 5451–5454.

(36) Guck, J.; et al. The optical stretcher: anovel laser tool to micromanipulate cells. *Biophys. J.* **2001**, *81*, 767–784.

(37) Chowdhury, A.; Ackerson, B. J.; Clark, N. A. Laser-induced freezing. *Phys. Rev. Lett.* **1985**, *55*, 833.

(38) Burns, M. M.; Fournier, J.-M.; Golovchenko, J. A. Optical binding. *Phys. Rev. Lett.* **1989**, *63*, 1233.

(39) Hu, W.; et al. Planar optical lattice of TiO_2 particles. *Opt. Lett.* **1995**, *20*, 964–966.

(40) Burns, M. B.; Fournier, J. M.; Golovchenko, J. A. Optical matter: crystallization and binding in intense optical fields. *Science* **1990**, *249*, 749.

(41) Garces-Chavez, V.; Dholakia, K.; Spalding, G. C. Extended-area optically induced organization of microparticles on a surface. *Appl. Phys. Lett.* **2005**, *86*, 031106.

(42) MacDonald, M. P.; Spalding, G. C.; Dholakia, K. Microfluidic sorting in an optical lattice. *Nature* **2003**, *426*, 421.

(43) Nieminen, T. A.; Parkin, S. J. W.; Heckenberg, N. R.; Rubinsztein-Dunlop, H. Optical torque and symmetry. *Proc. SPIE* **2004**, 254.

(44) Roichman, Y.; Sun, B.; Stolarski, A.; Grier, D. G. Influence of nonconservative optical forces on the dynamics of optically trapped colloidal spheres: the fountain of probability. *Phys. Rev. Lett.* **2008**, *101*, 128301.

(45) Sun, B.; Lin, J.; Darby, E.; Grosberg, A. Y.; Grier, D. G. Brownian vortexes. *Phys. Rev. E* **2009**, *80*, No. 010401.

(46) Arlt, J.; Garcés-Chávez, V.; Sibbett, W.; Dholakia, K. Optical micromanipulation using a Bessel light beam. *Opt. Commun.* **2001**, *197*, 239–245.

(47) Arlt, J.; Dholakia, K. Generation of high-order Bessel beams by use of an axicon. *Opt. Commun.* **2000**, *177*, 297–301.

(48) Chen, J.; Ng, J.; Lin, Z. F.; Chan, C. T. Optical pulling force. *Nat. Photonics* **2011**, *5*, 531–534.

(49) Novitsky, A.; Qiu, C. W.; Wang, H. Single gradientless light beam drags particles as tractor beams. *Phys. Rev. Lett.* **2011**, *107*, 203601.

(50) Sukhov, S.; Dogariu, A. Negative nonconservative forces: optical "tractor beams" for arbitrary objects. *Phys. Rev. Lett.* **2011**, *107*, 203602.

(51) Li, X.; Chen, J.; Lin, Z.; Ng, J. Optical pulling at macroscopic distances. *Sci. Adv.* **2019**, *5*, No. eaau7814.

(52) Brzobohatý, O.; Karasek, V.; Siler, M.; Chvatal, L.; Čižmár, T.; Zemánek, P. Experimental demonstration of optical transport, sorting and self-arrangement using a 'tractor beam'. *Nat. Photonics* **2013**, *7*, 123–127.

(53) Damková, J.; Chvatal, L.; Jezek, J.; Oulehla, J.; Brzobohatý, O.; Zemánek, P. Enhancement of the "tractor-beam" pulling force on an optically bound structure. *Light: Sci. Appl.* **2018**, *7*, 17135.

(54) Dogariu, A.; Sukhov, S.; Sáenz, J. Optically induced 'negative forces'. *Nat. Photonics* **2013**, *7*, 24–27.

(55) Chen, H.; Liu, S.; Zi, J.; Lin, Z. Fano resonance-induced negative optical scattering force on plasmonic. *ACS Nano* **2015**, *9* (2), 1926–1935.

(56) Galstyan, T. V.; Drnoyan, V. Light-driven molecular motor. *Phys. Rev. Lett.* **1997**, *78*, 2760.

(57) Liu, M.; Zentgraf, T.; Liu, Y.; Bartal, G.; Zhang, X. Light-driven nanoscale plasmonic motors. *Nat. Nanotechnol.* **2010**, *5*, 570.

(58) Donato, M. G.; et al. Optical trapping, optical binding, and rotational dynamics of silicon nanowires in counter-propagating beams. *Nano Lett.* **2019**, *19* (1), 342–352.

(59) Nieminen, T. A.; Asavei, T.; Loke, V. L. Y.; Heckenberg, N. R.; Rubinsztein-Dunlop, H. Symmetry and the generation and measurement of optical torque. *J. Quant. Spectrosc. Radiat. Transfer* **2009**, *110*, 1472.

(60) Sukhov, S.; Dogariu, A. Non-conservative optical forces. *Rep. Prog. Phys.* **2017**, *80*, 112001.

(61) Ashkin, A.; Gordon, J. P. Stability of radiation-pressure particle traps: an optical Earnshaw theorem. *Opt. Lett.* **1983**, *8*, 511–513.

(62) Ashkin, A. Forces of a single-beam gradient laser trap on a dielectric sphere in the ray optics regime. *Biophys. J.* **1992**, *61*, 569–582.

(63) Neuman, K. C.; Block, S. M. Optical trapping. *Rev. Sci. Instrum.* **2004**, *75*, 2787–2809.

(64) Wu, P.; Huang, R.; Tischer, C.; Jonas, A.; Florin, E. L. Direct measurement of the nonconservative force field generated by optical tweezers. *Phys. Rev. Lett.* **2009**, *103*, 108101.

(65) Albaladejo, S.; Marques, M. I.; Laroche, M.; Saenz, J. J. Scattering forces from the curl of the spin angular momentum of a light field. *Phys. Rev. Lett.* **2009**, *102*, 113602.

(66) Du, J.; Yuen, C. H.; Li, X.; et al. Tailoring optical gradient force and optical scattering and absorption force. *Sci. Rep.* **2017**, *7*, 18042.

(67) Wang, N.; Li, X.; Chen, J.; Lin, Z.; Ng, J. Gradient and scattering forces of anti-reflection-coated spheres in an aplanatic beam. *Sci. Rep.* **2018**, *8*, 17423.

(68) Jiang, Y.; Chen, J.; Ng, J.; Lin, Z. Decomposition of optical force into conservative and nonconservative components. *arXiv 1604.05138* **2016**, na.

(69) Bohern, C. F.; Huffman, D. R. *Absorption and Scattering of Light by Small Particles*; Wiley, 2008.